Percolation and jamming transitions in particulate systems with and without cohesion

L. Kovalcinova, A. Goullet, and L. Kondic
Department of Mathematical Sciences, New Jersey Institute of Technology, University Heights, Newark, New Jersey 07102, USA
(Received 15 February 2015; published 30 September 2015)

We consider percolation and jamming transitions for particulate systems exposed to compression. For the systems built of particles interacting by purely repulsive forces in addition to friction and viscous damping, it is found that these transitions are influenced by a number of effects, and in particular by the compression rate. In a quasistatic limit, we find that for the considered type of interaction between the particles, percolation and jamming transitions coincide. For cohesive systems, however, or for any system exposed to even slow dynamics, the differences between the considered transitions are found and quantified.

DOI: 10.1103/PhysRevE.92.032204 PACS number(s): 45.70.−n, 64.70.qj, 81.05.Rm, 82.70.−y

I. INTRODUCTION

The dense systems of particles interacting by either purely repulsive potentials, such as dry granular particles, or by both repulsive and attractive ones, such as wet granulates, appear virtually everywhere, from nature to a variety of applications bridging the scales from nano to macro. The structure of the force field by which the particles interact may be very complex, in particular on mesoscales where this force field is nonuniform and forms force networks. These networks are of relevance not only to granular systems, but to many others, such as foams and colloids. Their properties have recently been explored using a variety of different approaches, ranging from theoretical and computational properties based on exploring the local structure of force networks [1] to network types of approaches [2,3] and topological methods [4–6].

While percolation has been considered for dense particulate systems [7–10], much more is known about static and ordered lattice-based systems [11,12], for which two types of percolation are discussed—rigidity and connectivity percolation [13,14]. However, lattice models do not account for nonlinear effects at particle contacts, such as friction and viscous damping, or for dynamics, so it is unclear whether the results obtained for lattice systems apply to particulate ones [14]. For the latter, the connection between percolation (connectivity) and jamming (rigidity) transitions was discussed recently for both noncohesive and cohesive frictionless systems, and it was found (for the systems considered) that these two transitions differ in general [9,10]. However, these conclusions were reached by considering rather specific interaction models (overdamped dynamics), and the question of whether they hold in general, and whether they also follow from the models commonly used to simulate physical granular particles, is still open.

In this paper, we discuss the relation between percolation and jamming for frictional and frictionless particles in two spatial dimensions, both with and without cohesion. We consider slowly compressed systems that go through percolation and jamming, and we discuss how these transitions depend on the system properties. The motivation for considering compression is that it is a simple protocol that avoids the complexities associated with shear, and it allows us to focus the discussion. However, consideration of any dynamics, including compression, naturally leads to the questions related to the rate dependence of the results, and, as we will see, to new insight into percolation and jamming transitions for evolving particulate systems.

The paper is organized as follows. In Sec. II we present the simulation techniques. In Sec. III we present out findings, first for purely repulsive systems in Sec. III A, and then for cohesive ones in Sec. III B. Section IV is devoted to a summary, conclusions, and future outlook.

II. SIMULATIONS

We perform discrete element simulations using a set of circular particles confined in a square domain, using a slow-compression protocol [4,5], augmented by relaxation as described below. Initially, the system particles are placed on a square lattice and are given random velocities; we have verified that the results are independent of the distribution and magnitude of these initial velocities. The discussion related to possible development of spatial order as the system is compressed can be found in [5], and the issue of spatial isotropy of the considered systems is considered later in the text.

In our simulations, gravity is not considered, and the diameters of the particles are chosen from a flat distribution of width r_p. System particles are soft inelastic disks and interact via normal and tangential forces, including static friction, μ (as in [4,5]). The particle-particle (and particle-wall) interactions include normal and tangential components. The normal force between particles i and j is

$$\begin{aligned} \mathbf{F}^n_{i,j} &= k_n x \mathbf{n} - \gamma_n \bar{m} \mathbf{v}^n_{i,j}, \\ r_{i,j} &= |\mathbf{r}_{i,j}|, \quad \mathbf{r}_{i,j} = \mathbf{r}_i - \mathbf{r}_j, \quad \mathbf{n} = \mathbf{r}_{i,j}/r_{i,j}, \end{aligned} \tag{1}$$

where $\mathbf{v}^n_{i,j}$ is the relative normal velocity. The amount of compression is $x = d_{i,j} - r_{i,j}$, where $d_{i,j} = (d_i + d_j)/2$, and d_i and d_j are the diameters of the particles i and j. All quantities are expressed using the average particle diameter, d_{av}, as the length scale, the binary particle collision time $\tau_c = 2\pi\sqrt{d_{\mathrm{av}}/(2gk_n)}$ as the time scale, and the average particle mass m as the mass scale. $\bar{m}$ is the reduced mass, k_n (in units of mg/d_{av}) is set to a value corresponding to photoelastic disks [15], and γ_n is the damping coefficient [16]. The parameters entering the linear force model can be connected to physical properties (Young modulus, Poisson ratio) as described, e.g., in [16].

We implement the commonly used Cundall-Strack model for static friction [17], where a tangential spring is introduced between particles for each new contact that forms at time $t = t_0$. Due to the relative motion of the particles, the spring length, $\boldsymbol{\xi}$, evolves as $\boldsymbol{\xi} = \int_{t_0}^{t} \mathbf{v}_{i,j}^{t}(t')dt'$, where $\mathbf{v}_{i,j}^{t} = \mathbf{v}_{i,j} - \mathbf{v}_{i,j}^{n}$. For long-lasting contacts, $\boldsymbol{\xi}$ may not remain parallel to the current tangential direction defined by $\mathbf{t} = \mathbf{v}_{\mathbf{i,j}}^{\mathbf{t}}/|\mathbf{v}_{\mathbf{i,j}}^{\mathbf{t}}|$ (see, e.g., [18]); we therefore define the corrected $\boldsymbol{\xi}' = \boldsymbol{\xi} - \mathbf{n}(\mathbf{n}\cdot\boldsymbol{\xi})$ and introduce the test force

$$\mathbf{F}^{t*} = -k_t\boldsymbol{\xi}' - \gamma_t\bar{m}\mathbf{v}_{i,j}^{t}, \tag{2}$$

where γ_t is the coefficient of viscous damping in the tangential direction (with $\gamma_t = \gamma_n$). To ensure that the magnitude of the tangential force remains below the Coulomb threshold, we constrain the tangential force to be

$$\mathbf{F}^{t} = \min(\mu|\mathbf{F}^{n}|, |\mathbf{F}^{t*}|)\mathbf{F}^{t*}/|\mathbf{F}^{t*}| \tag{3}$$

and redefine $\boldsymbol{\xi}$ if appropriate.

Cohesive forces are modeled using the approach outlined in [19], and they are considered to arise from the capillary bridges that form when particles come into contact. The functional form of this force is given by

$$F_b = 2\pi R\gamma\cos\theta/(1 + 1.05\hat{s} + 2.5\hat{s}^2), \tag{4}$$

where $\hat{s}{=}s\sqrt{R/V}$, and $s{=}r_{ij}{-}(d_i + d_j)/2$ (taken to be $\geqslant 0$) is the particle separation. Here, $1/R = 1/2(1/d_1 + 1/d_2)$ [20] (for simplicity, we do not account here for polydispersity and use $d_1 = d_2 = 1$ in dimensionless units), and V is the volume of a capillary bridge between particles. In the present work, we assume that all capillary bridges are of the same volume. For contact angle, θ, we use $\theta = 12^\circ$, comparable to the value for (deionized ultrafiltered) water and (clean) glass [21]. For the surface tension, γ, we use the value corresponding to water, 72 dyn/cm, scaled appropriately. The critical separating distance, s_c, at which a bridge breaks is given by

$$s_c = (1 + \theta/2)(V^{1/3}/R + V^{2/3}/R^2). \tag{5}$$

Here, s_c could be thought of as a measure of the strength of cohesion; larger s_c leads to more pronounced cohesive effects.

Our simulations are carried out by slowly compressing the domain, starting at the packing fraction 0.63 and ending at 0.90, by the moving walls built of monodisperse particles with diameters of size d_{av} placed initially at equal distances, d_{av}, from each other. The wall particles move at a uniform (small) inward velocity, v_c, equal to $v_0 = 2.5{\times}10^{-5}$ (in the units of d_{av}/τ_c), or a fraction of it, as we explore the influence of compression speed. Due to compression and uniform inward velocity, the wall particles (that do not interact with each other) overlap by a small amount. When the effect of compression rate is explored, v_c is decreased, or the compression is stopped to allow the system to relax. To obtain statistically relevant results, we simulate a large number of initial configurations (typically 20), and we average the results. Due to the compression being slow, we do not observe any different behavior close to the domain boundaries compared to the rest of the domain.

We integrate Newton's equations of motion for both the translational and rotational degrees of freedom using a fourth-order predictor-corrector method with time step $\Delta t = 0.02$. Our reference system is defined by $N = 2000$ polydisperse particles ($r_p = 0.2$), with $k_n = 4{\times}10^3$, $e_n = 0.5$, $\mu = 0.5$, and $k_t = 0.8k_n$ [22]; the (monodisperse) wall particles have the same physical properties. Larger domain simulations are carried out with up to $N = 20\,000$ particles. If not specified otherwise, cohesion is not included.

III. RESULTS

A. Purely repulsive systems

Figure 1(a) shows an example of the reference system at $\rho = 0.90$, with the particles color-coded according to the total normal force, normalized by the average normal force, $F_n/\langle F\rangle$ (we focus only on the normal forces in the present work). If the system contains a set of particles in contact that connects top/bottom or left/right wall, then there is contact percolation. We will also consider force percolation by focusing on the particles sustaining a force larger than a given force threshold and ask how the percolation properties are influenced by a nonvanishing threshold.

As an example, Fig. 1(b) shows the same system as in Fig. 1(a) with force threshold $\bar{F} = 1$. While the system shown in Fig. 1(a) clearly percolates (contact percolation), it is not immediately obvious whether the system shown in Fig. 1(b) does.

In describing percolation properties, we use the following quantities, all based on averaging over multiple realizations: $P(\rho,\bar{F})$, the percolation probability; $\bar{F}_p$, the percolation force threshold, defined by $P(\rho,\bar{F}_p) = 0.5$; and $P_c(\rho)$, the contact percolation probability, defined as $P_c(\rho) = P(\rho,0)$. In addition, we will use Z, the coordination number, measuring the average number of contacts per particle; a sharp increase of the Z curve is typically associated with the jamming transition; see, e.g., [23]. We note that the listed quantities also depend on the number of particles, N, and on the compression speed, v_c; this dependence will be discussed later in the paper. For simplicity of notation, we do not include this dependence explicitly in the notation.

Figure 2(a) shows $P(\rho,\bar{F})$ for the reference system. We see that, starting at $\rho \approx 0.77$, there is a percolation transition; note that if we vary $\bar{F}$ and keep ρ fixed, this transition is rather sharp for large ρ's and more spread out for $\rho \in [0.77,0.81]$. To describe various transitions that take place as the system is compressed, we define the following: ρ_J, at which jamming, defined here as the ρ at which the Z curve has an inflection

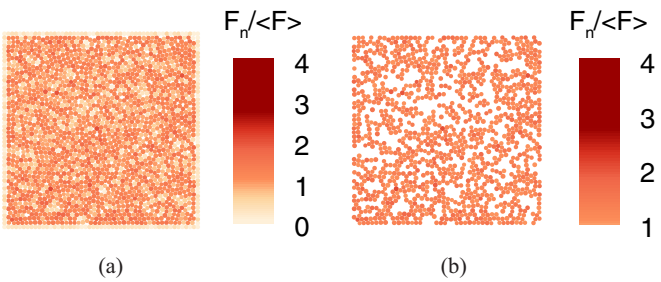

FIG. 1. (Color online) An example of a reference system for different force thresholds at $\rho = 0.9$ (see the Supplementary Material in Ref. [4] for animations). (a) $\bar{F} = 0$, (b) $\bar{F} = 1$.

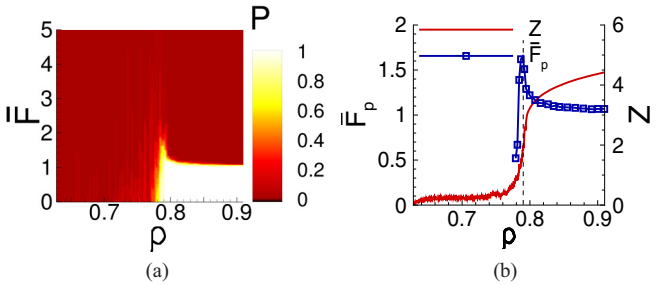

FIG. 2. (Color online) Reference system, averaged over 20 realizations. (a) The percolation probability, $P(\rho,\bar{F})$; (b) the percolation force threshold, $\bar{F}_p$, and the coordination number, Z.

point, takes place (later in the text, we also show that at ρ_J a rapid increase in pressure (measured at the domain boundaries) occurs, supporting this definition of ρ_J); and ρ_p, at which contact percolation, defined as $P_c(\rho_p) = 0.5$, occurs. Figure 2(b) shows Z and $\bar{F}_p$; we find from the data shown that $\rho_J \approx 0.79$ (the vertical dashed line in the figure). Note that just below ρ_J, there is a strong force network that percolates, as shown by large $\bar{F}_p$. The dominant maximum of $\bar{F}_p$ calls for consideration of another transitional ρ at which this maximum occurs: however, we find that this transition is always sandwiched between ρ_p and ρ_J, so we will not discuss it in more detail here.

Figure 3(a) shows Z and P_c for the reference system. While there is some noise in the results, one can still obtain an accurate value for $\rho_p \approx 0.776$. [For this and all other results involving ρ_p and ρ_J, uncertainty of the results is such that the results are accurate up to three significant digits: for ρ_J we use standard error to estimate uncertainty, and for ρ_p we estimate the range over which $0.4 \leqslant P_c(\rho) \leqslant 0.6$.] Therefore, the results for our reference system suggest that $\rho_p < \rho_J$, and the question is whether this finding is robust with respect to the changes of the system parameters and of the protocol used. Before proceeding, we note that although there are some differences between realizations, for all of them we find consistently (for the considered system) that ρ_p and ρ_J differ by a nonvanishing amount.

Regarding the system parameters, we start by discussing the influence of polydispersity, measured by r_p, and the friction coefficient, μ. Table I shows the results for ρ_p and ρ_J, and we observe that both ρ_p and ρ_J are monotonously decreasing functions of these two parameters; in particular, the results for

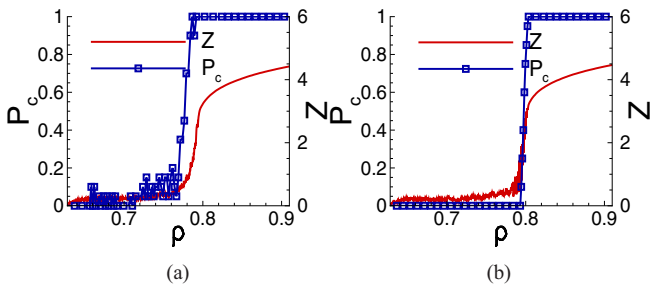

FIG. 3. (Color online) Reference system: the percolation probability, P_c, and Z. (a) $v_c = v_0$; (b) $v_c = 0$.

TABLE I. Influence of μ, r_p, and v_c on ρ_p and ρ_J for a continuously compressed system (the parameters not specified correspond to the reference case).

	μ					
	0.0	0.1	0.2	0.3	0.4	0.5
ρ_J	0.827	0.812	0.802	0.797	0.796	0.789
ρ_p	0.815	0.799	0.792	0.784	0.781	0.776
	r_p					
	0.0	0.1	0.2	0.3	0.4	
ρ_J	0.804	0.797	0.789	0.7834	0.782	
ρ_p	0.786	0.784	0.776	0.771	0.766	
	v_c/v_0					
	0.0	0.02	0.05	0.1	1.0	
ρ_J	0.798	0.799	0.798	0.792	0.789	
ρ_p	0.798	0.794	0.791	0.786	0.776	

ρ_J are consistent with those from the literature (see [4] and references therein). The finding that is perhaps more relevant for the present discussion is that the difference between ρ_p and ρ_J remains as r_p and μ are varied.

Next we discuss the influence of system size; note that this issue has been discussed extensively in the context of random percolation (see, e.g., [11]). Here, the context is more complicated since the system considered is dynamic, and one has to decide on coupling of relevant spatial and temporal scales. We have considered two scenarios for systems of different size: one in which the rate of change of ρ is kept constant, and one in which the compression speed (v_c) is fixed. While the details of the results vary depending on the choice of scenario, we find that the difference between ρ_p and ρ_J remains nonzero (and typically increases as a function of L) for both scenarios and for the system sizes defined by $L = 50, 75, 100, 150$: Figure 4 shows the dependence of ρ_p and ρ_J behavior on the system size using the two aforementioned protocols. Figure 4(a) shows results for the fixed compression rate; the compression velocity, v_c, is increased with L so that the rate v_c/L is constant. Figure 4(b) shows ρ_p, ρ_J when we keep v_c constant as L increases. For both protocols—

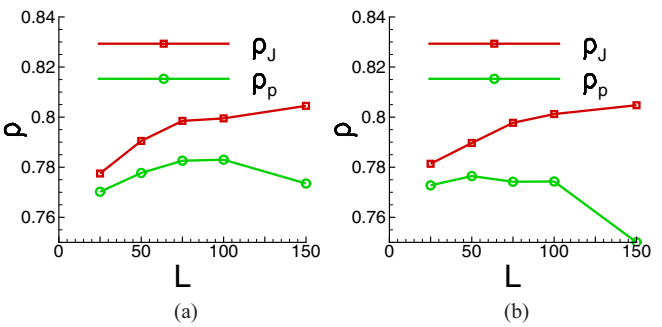

FIG. 4. (Color online) Influence of system size on ρ_p and ρ_J for a fixed compression rate and a fixed compression speed. (a) Fixed compression rate; (b) fixed compression speed.

fixed compression rate and speed—we observe an increased difference between ρ_p and ρ_J as L is increased.

Since the reference system is exposed to a nonvanishing compression rate, there is also the question of rate dependence, as already alluded to above. To explore this issue, we carry out simulations with progressively slower compression, using $v_c = v_0/10$, $v_0/20$, and $v_0/50$. We find that the P_c transition becomes sharper as v_c decreases, indicating that ρ_p is affected by v_c; in general, for a fixed ρ, the particles are less likely to percolate for smaller v_c and therefore ρ_p increases as v_c decreases. Both ρ_p and ρ_J are shown in Table I. While both ρ's increase as v_c decreases, the crucial finding is that the difference between them becomes smaller for slower compression. The question remains whether ρ_p and ρ_J collapse to a single value in the limit $v_c \to 0$. To answer this, we consider a modified protocol such that we interject relaxation steps in our compression (we reference this protocol by $v_c = 0$). More precisely, after compressing the system by $\delta\rho = 0.001$, we check whether there is a percolating cluster. If not, we proceed with compression; if yes, the system is relaxed until percolation disappears, and then the system is further compressed. We carry out this procedure until such ρ_p that the percolating cluster does not disappear after relaxation (for all considered simulations, the system always percolates above ρ_p found using the relaxation protocol, or in other words, percolation is never found to disappear as a system is further compressed). Figure 3(b) shows P_c and Z for the relaxed system, suggesting much smoother and sharper evolution of P_c through ρ_p. Table I shows that for the reference system and $v_c = 0$, ρ_p and ρ_J collapse to the same point, within the available accuracy. We have reached the same finding for the other systems listed in Table I, including monodisperse frictionless system—while this particular system is known to show different behavior due to partial crystallization [4], it still leads to $\rho_p = \rho_J$. We have also verified that the finding $\rho_p = \rho_J$ still holds when different system sizes are considered.

This finding of collapse of percolation and jamming transitions appears to be different from that in [10], where it was found that ρ_p and ρ_J differ. The source of the difference seems to be the use of overdamped dynamics in [10]; this effect apparently keeps the particles together and leads to percolation even for small ρ's. We find, however, that, within the particle interaction model considered in the present paper, based on a (constant) coefficient of restitution, e_n, the finding $\rho_p = \rho_J$ persists even for very small $e_n \approx 0$, suggesting that the finding reported here is robust, within the framework of the implemented particle interaction model.

While the findings obtained in the quasistatic limit are of primary interest, one should note that in the context of particulate matter, percolation and jamming transitions typically involve dynamics, even if very slow. Close to ρ_J, the relevant time scales diverge in the limit of infinite system size, and therefore one could expect that for any sufficiently large system, even very slow dynamics may lead to (arbitrarily small) differences between ρ_p and ρ_J. Therefore, it should not be surprising if differences are found between ρ_p and ρ_J for slowly evolving spatially extended particulate systems.

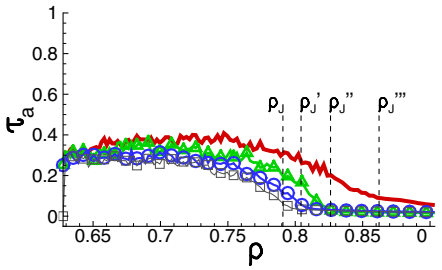

FIG. 5. (Color online) Anisotropy of the stress tensor of r_p=0.2, $\mu = 0.5$ (squares), $r_p = 0.0, \mu = 0.5$ (circles), $r_p = 0.2, \mu = 0.0$ (triangles), and $r_p = 0.0, \mu = 0.0$ (thick line) systems as a function of packing fraction, ρ. Respective jamming transitions, $\rho_J, \rho_J', \rho_J'', \rho_J'''$, are depicted by a dashed line.

To close our discussion focusing on repulsive systems, we discuss whether the implemented compression protocol may induce anisotropy, possibly influencing the results. For this purpose, we compute the stress tensor and the distribution of the angles of contact between the particles. For brevity, we consider here only the compression by v_0. The stress anisotropy, τ_a, is defined by

$$\tau_a = \frac{\sigma_1 - \sigma_2}{\sigma_1 + \sigma_2} \tag{6}$$

with σ_1, σ_2 the principal eigenvalues of the Cauchy stress tensor σ, specified by $\sigma_{ij} = 1/(2A) \sum_{c_k,p} (F_i r_j + F_j r_i)$ as a sum over all interparticle contacts c_k for all particles p (wall particles as well as the contacts of interior particles with the wall particles are not included here). Here, A is the total area of the system, and r_i, r_j are the x and y components of the vector pointing from the center of particle p toward the particle contact c_k. F_i, F_j denote the x,y components of the interparticle force at the contact c_k.

Figure 5 shows τ_a as a function of ρ. We depict jamming transitions ρ_J, ρ_J', ρ_J'', and ρ_J''' by dashed lines for $\mu = 0.5, r_p = 0.2$ (reference system); $\mu = 0.5, r_p = 0.0$; $\mu = 0.0, r_p = 0.2$; and $\mu = 0.0, r_p = 0.0$; respectively. While far below the jamming (and percolation) transitions the anisotropy measured by τ_a may be present, close to ρ_p and ρ_J, $\tau_a \ll 1$ for all systems considered, showing that the systems are essentially isotropic for the packing fractions of relevance here. Above jamming points, τ_a is even smaller.

Figure 6 shows the distribution of the contact angle, ϕ, for the reference system [Figs. 6(a) and 6(b)], and for the $\mu = 0.0$, $r_p = 0.0$ system [Figs. 6(c) and 6(d)]. Most importantly, this figure shows a symmetric distribution of ϕ's. In addition, by comparing the results of the reference case with those obtained for the monodisperse frictionless case, we also observe the influence of partial crystallization on the latter for large packing fractions.

B. Cohesive systems

Here, we discuss the effect of cohesion on percolation and jamming. We have considered a few different "strengths" of cohesion (specified by the distance, s_c) at which capillary bridges break; for brevity here we present results only for "weak" cohesion, specified by the small distance at which

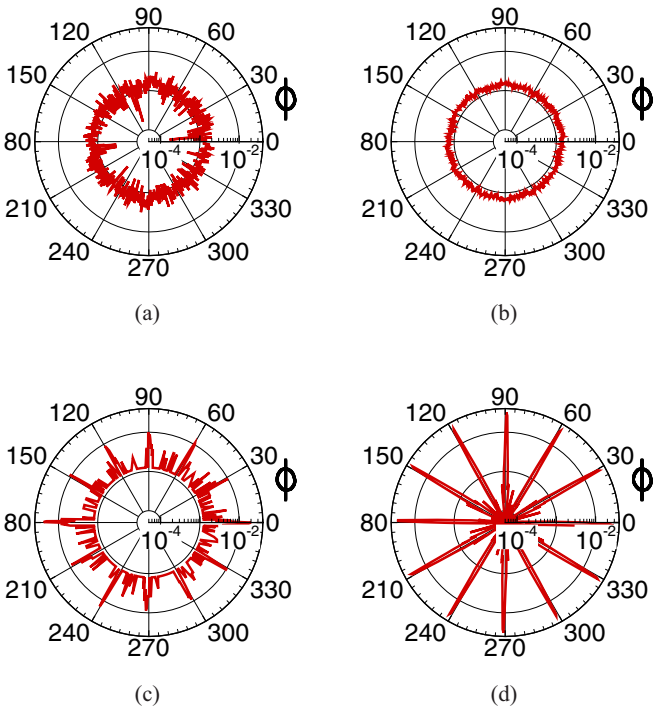

FIG. 6. (Color online) Distribution of the angles of contacts for the reference (a),(b) and the $r_p = 0.0, \mu = 0.0$ system (c),(d). In these polar plots, the azimuthal coordinate, ϕ, corresponds to the angle between the line connecting the centers of contacting particles and the $+x$ axis, and the radial one to the probability of observing given ϕ. (a) $\rho = 0.73$; (b) $\rho = 0.90$; (c) $\rho = 0.73$; (d) $\rho = 0.90$.

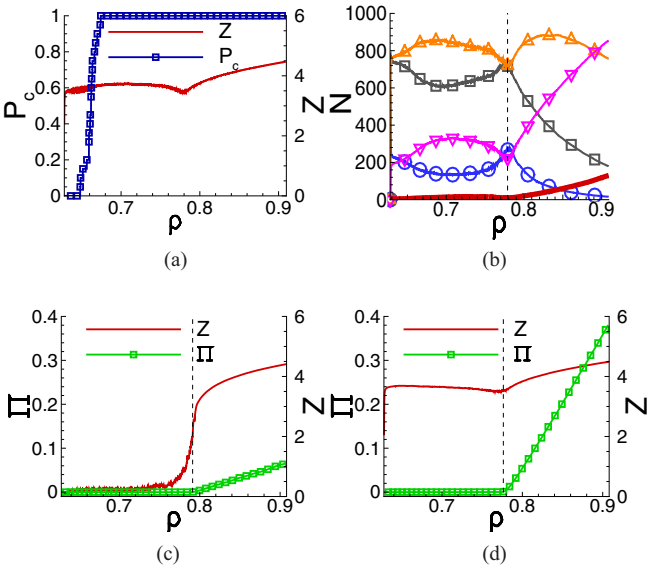

FIG. 7. (Color online) (a),(b) Cohesive relaxed system. (c),(d) Pressure on the walls, Π, and Z. Dashed lines correspond to ρ_J [and to ρ_p in (c)]; in (a), ρ_p is shown by a dotted line. (a) P_c and Z; (b) number of particles with $cn = 2$–6 contacts (circle, square, triangle, gradient, and thick line, consecutively); (c) reference relaxed system; (d) cohesive relaxed system.

capillary bridges break, $s_c \approx 0.0028 \ll 1$ (see Sec. II). We focus on the relaxed reference system. Figure 7(a) shows that the percolation transition occurs very close to (the starting value) $\rho = 0.63$. The Z curve remains at high values for all considered ρ's, but we note that there is a kink in the Z curve at $\rho \approx 0.783$. The kink and consecutive increase of Z suggest that the system undergoes a transition. To verify that this transition corresponds to ρ_J, we consider the pressure on the system walls, Π. Figures 7(c) and 7(d) shows this pressure (force/length, in dimensionless units) for both the reference system and the cohesive one. We see that for the reference system, an increase of Π occurs at ρ_J (inflection point of the Z curve). Figure 7(d) shows that an increase in Π and the kink in the Z curve occur at the same $\rho = \rho_J = 0.783$.

Clearly, the difference between ρ_J and ρ_p is significant for the considered cohesive system, consistent with the earlier work [9]. As expected, we find similar results for the systems characterized by larger s_c (results not shown for brevity). The strong influence of weak cohesion on ρ_p and ρ_J suggests that for any nonvanishing cohesion, one would find differences between ρ_P and ρ_J, with these differences disappearing only in the limit of $s_c \to 0$. As soon as there is no attractive force, the difference between ρ_p and ρ_J vanishes even in the limit of inelastic collisions, $e_n \to 0$.

One may ask about the origin of the "kink" in the Z curves for the cohesive system. An intuitive explanation is as follows: as compression starts, the particles immediately come into contact with each other and form miniclusters (consisting of a small number of particles), leading to rather large Z; due to the presence of cohesive forces, relaxation does not lead to the breakup of the existing contacts. Therefore, as long as ρ is small, the miniclusters do not break; as ρ grows, however, collisions start separating particles, leading to breakup of the miniclusters and decreasing Z. At some point, when ρ becomes sufficiently large so that all particles are effectively in contact, Z starts growing again, and at the same ρ, Π starts increasing. To support this description, Fig. 7(b) shows the number of particles (N) with $2, \ldots, 6$ contacts (cn). We observe that as ρ_J is approached from below, the $cn = 4,5$ curves have a negative slope, suggesting breakup of the clusters (this breakup is presumably also partially responsible for the positive slope of $c_n = 2,3$ curves for the same values of ρ); at ρ_J, these trends reverse.

IV. SUMMARY AND CONCLUSIONS

Percolation and jamming transitions of evolving particulate systems are nontrivial. We find that these transitions for repulsive particles interacting by a commonly used interaction model coincide for quasistatic systems; this finding, together with the results reported in [10], where these transitions are found to differ for particles following overdamped dynamics, suggests that the considered transitions may be influenced significantly by the type of interaction between the particles. Furthermore, our finding is that any, even very slow, dynamics may lead to the differences of the packing fractions at which percolation and jamming occur. Therefore, in particular close to jamming, a careful exploration will be needed in order to distinguish the effects due to dynamics and due to, e.g., the type of interaction between the particles. In the same vein, we

are also finding that even minor cohesive effects have a strong influence in particular on percolation transition.

We hope that the present results will encourage carrying out careful experiments that will quantify further the predictions regarding the influence that dynamics, cohesion, and the nature of particle interaction have on percolation and jamming. Our own research will continue in the direction of exploring the effects of jamming and percolation in three spatial dimensions.

ACKNOWLEDGMENT

This work was partially supported by NSF Grant No. DMS-0835611.

[1] J. F. Peters, M. Muthuswamy, J. Wibowo, and A. Tordesillas, Phys. Rev. E **72**, 041307 (2005).
[2] D. S. Bassett, E. T. Owens, K. E. Daniels, and M. A. Porter, Phys. Rev. E **86**, 041306 (2012).
[3] M. Herrera, S. McCarthy, S. Slotterback, E. Cephas, W. Losert, and M. Girvan, Phys. Rev. E **83**, 061303 (2011).
[4] L. Kondic, A. Goullet, C. O'Hern, M. Kramar, K. Mischaikow, and R. Behringer, Europhys. Lett. **97**, 54001 (2012).
[5] M. Kramar, A. Goullet, L. Kondic, and K. Mischaikow, Phys. Rev. E **87**, 042207 (2013).
[6] R. Arévalo, L. A. Pugnaloni, I. Zuriguel, and D. Maza, Phys. Rev. E **87**, 022203 (2013).
[7] E. Aharonov and D. Sparks, Phys. Rev. E **60**, 6890 (1999).
[8] R. Arévalo, I. Zuriguel, and D. Maza, Phys. Rev. E **81**, 041302 (2010).
[9] G. Lois, J. Blawzdziewicz, and C. S. O'Hern, Phys. Rev. Lett. **100**, 028001 (2008).
[10] T. Shen, C. S. O'Hern, and M. D. Shattuck, Phys. Rev. E **85**, 011308 (2012).
[11] D. Stauffer and A. Aharonov, *Introduction to Percolation Theory* (Taylor & Francis, Philadelphia, 2003).
[12] R. Albert and A.-L. Barabási, Rev. Mod. Phys. **74**, 47 (2002).
[13] S. Alexander, Phys. Rep. **296**, 65 (1998).
[14] E. Guyon, S. Roux, and A. Hansen, Rep. Prog. Phys. **53**, 373 (1990).
[15] J. Geng, R. P. Behringer, and G. Reydellet, Physica D **182**, 274 (2003).
[16] L. Kondic, Phys. Rev. E **60**, 751 (1999).
[17] P. A. Cundall and O. D. L. Strack, Géotechnique **29**, 47 (1979).
[18] L. Brendel and S. Dippel, in *Physics of Dry Granular Media* (Kluwer Academic, Dordrecht, 1998), p. 313.
[19] S. Herminghaus, Adv. Phys, **54**, 221 (2006).
[20] C. Willett, M. Adams, S. Johnson, and J. Seville, Langmuir **16**, 9396 (2000).
[21] Y. Gu, in *Encyclopedia of Surface and Colloid Science*, 2nd ed., edited by P. Somasundaran (Taylor & Francis, New York, 2006), Vol. 4, pp. 2711–2721.
[22] C. Goldenberg and I. Goldhirsch, Nature (London) **435**, 188 (2005).
[23] T. S. Majmudar, M. Sperl, S. Luding, and R. P. Behringer, Phys. Rev. Lett. **98**, 058001 (2007).